Effect of TiO_2 Nanoparticles on the Horizontal Hardness Properties of Sn-3.0Ag-0.5Cu-1.0TiO_2 Composite Solder

Siti Shareeda Mohd Nasir[1], Muhamad Zamri Yahaya[2], Ahmet Mustafa Erer[3], Balázs Illés[4] and Ahmad Azmin Mohamad[2,*]

[1]Fakulti Kejuruteraan Mekanikal, Universiti Teknologi Mara, Cawangan Pulau Pinang Kampus Permatang Pauh, Jalan Permatang Pauh, 13500 Permatang Pauh | Pulau Pinang

[2]School of Materials and Mineral Resources Engineering, Universiti Sains Malaysia, 14300 Nibong Tebal, Pulau Pinang, Malaysia

[3]Department of Physics, Karabuk University, 78200 Karabuk, Turkey

[4]Department of Electronics Technology, Budapest University of Technology and Economics, Budapest, Hungary

*Corresponding author: aam@usm.my

Abstract

The improvement in the hardness of Sn-3.0Ag-0.5Cu solder alloy reinforced with 1.0 wt. % TiO_2 nanoparticles was evaluated by nanoindentation. A specific indentation array was performed on four different horizontal cross sections of the composite solder with different heights and diameters, in order to verify the mixing homogeneity of TiO_2 nanoparticles within the Sn-3.0Ag-0.5Cu solder paste during the ball milling process. The phase analysis indicated successful blending of the Sn-3.0Ag-0.5Cu with the TiO_2 nanoparticles. According the scanning electron microscopy micrographs, presence of the TiO_2 nanoparticles reduced the size of the Cu_6Sn_5 and Ag_3Sn intermetallic compound phases. Incorporation of the 1.0 wt. % TiO_2 nanoparticles improved the hardness values up to 26.2 % than that of pure SAC305. The hardness values increased gradually from the top cross sections towards adjacent to the solder/substrate interface. The mechanism of the hardness improvement attained by the TiO_2 nanoparticles addition were also investigated on the horizontal cross sections of the samples.

Keywords: nanoindentation; composites; soldering; SAC, grain refinement

1. Introduction

Nowadays, ternary Sn–Ag–Cu (SAC) lead-free solder alloys have been mostly used in most of electronic assemblies [1, 2]. However, large volume fraction of Ag_3Sn intermetallic compound (IMC) and its fast reaction rate with the metallization layer is still the main drawback of the SAC solders [3]. The formation and growth of the IMC layer is more rapid in

SAC solder joints than it was in lead contain alloys, and it results in not only brittle fractures but also reduces the thermal fatigue life of the joints [4]. One of the recent approach, which can address this issue is to develop a nano-composite solders with the incorporation of a small amount of metallic or ceramic nanoparticles into the SAC solder. The incorporation of nanoparticles provided significant improvements about morphological [5, 6] thermal behaviour [7-9], and mechanical properties [10, 11] of the SAC solders. Non-reacting and non-coarsening oxide dispersoids such as ZrO_2 [6, 12], Al_2O_3 [13, 14], ZnO [5], SiC [15, 16] and TiO_2 [17, 18] were identified as potential reinforcement materials [3, 7]. Additionally, the properties of TiO_2 (like low cost and easy production) makes this ceramic the most promising candidate to produce SAC composite solder alloys.

The addition of TiO_2 nanoparticles significantly improve the mechanical properties of the SAC. The incorporation of 0.1 wt. % TiO_2 nanoparticles resulted in a 37 % increase of the microhardness value [5], and the maximum improvement of the hardness even reached 16.4 Hv (0.1608 GPa) in the case of Sn-3.5Ag-0.5Cu (SAC355) alloy with 1.0 wt. % TiO_2 nanoparticles [6]. The improvements of the mechanical properties were caused by the refined β-Sn, Cu_6Sn_5 and Ag_3Sn IMC phases. The hardness evaluation of lead-free solder alloys are usually carried out with a direct indentation on the top solder bump/joint (**Figure 1a).** The morphological alteration factor (which improves the hardness) has high correlation with the distribution of the reinforcement particles; whereas the TiO_2 nanoparticles are favourably distributed close to the IMC layer of the SAC305 solder joints [19]. Since, the distribution of the nanoparticles is also influenced by the gravitational force, most of the studies are conducted with vertical indentation procedure (**Figure 1b**). However, similar information can also be gained by the multiple horizontal indentation on cross-sections (**Figure 1c**). By engaging the use of high resolution nanoindentation testing, a specific indentation path can be reached to get essential information, how the reinforcement particles affect the horizontal hardness (**Figure 1d**).

In this study, different horizontal cross-sections of the SAC305 solder with TiO_2 nanoparticles were prepared and evaluated with nanoindentation. Phase analysis, morphological observation, elemental determination as well as the characterization of the different cross-sections were also conducted in order to understand and describe the way of the hardness improvement.

2. Experimental

2.1 Preparation of the SAC305 composite solder

The Sn-3.0Ag-0.5Cu-TiO_2 (SAC305-1.0T) composite solder was prepared from the ALPHA CVP-390 (Alpha Assembly Solutions) solder paste with addition of 1.0 wt. % sol-gel synthesized TiO_2 reinforcement nanoparticles (16.65 nm) [7]. They were ball milled for 10 minutes using a planetary ball mill (Pulverisette 5, Fritsch) with a rotational speed of 300 rpm.

Solder paste was printed trough an aluminium stencil with a 5 mm diameter and a 1 mm thickness onto a 2 cm × 3 cm FR4 substrate (Destiny Electronics). Solder paste was reflowed by a convection reflow oven (TYR-108C, Madell Technology) with the following profile: preheating (80 s, 160–180 °C), reflowing (40 s, 213–247 °C), and cooling (200 s, 247–40 °C). Four horizontal cross sections were subsequently prepared according to the given heights and diameters of the solder bumps in **Table 1**. The preparation of the cross-sections was the following: the solder bumps were grinded using 800 grit silicon carbide paper still the given height was reached, then the cross-sections were refined using 1200 and 2000 grit silicon carbide papers. Finally, the cross-sections were polished with the use of 1.0, 0.5, and 0.03 µm alumina suspensions.

2.2 Characterization of the SAC305 composite solder alloy

The phase analysis on both SAC305 and SAC305-1.0T were conducted by X-ray diffraction (XRD, Bruker AXS D9) with monochromatized Cu Kα radiation (λ = 1.5406 Å) over a range of $10° < 2\theta < 90°$. The morphological observations were done with a Field-Emission Scanning Electron Microscope (FESEM, 35VP, Zeiss SupraTM) equipped with Energy Dispersive X-ray (EDX). Nanoindeter (NanoTest Vantage, Micro Materials) with triangular Berkovich tip was used to measure the hardness level. The indentation was done with maximum load of 50 mN, loading rate was 1 mN s^{-1} and dwell time was 50 s. A series of indentation patterns were applied according to the diameter of the given cross-section, the average indentation gap was -50 µm (**Figure 2**).

3. Results and Discussion

3.1 Structural and phase analysis

The International Centre of Structural Data (ICSD) was used to determine the initial phases on the normalized XRD patterns of the SAC305 and SAC305-1.0T solder alloys (**Figure 3a-b**). Upon the solidification, three different phases were detected in the SAC305 solder, namely the β-Sn (ICSD-98-009-1748), Cu_6Sn_5 (ICSD-98-010-9332) and Ag_3Sn (ICSD-98-000-1559). The TiO_2 (ICSD-98-000-5226) were subsequently detected at $2\theta = 37.81°$ but only in SAC305-1.0T. The peak intensities of identified phases increased significantly towards

the inner cross-sections in both cases. Generally, the SAC305-1.0T alloy, demonstrated higher peak intensities than the SAC305. The addition of the TiO_2 nanoparticle did not have significant influences on the peak positioning of the identified phases.

The XRD results proved that the inclusion of TiO_2 nanoparticles did not result in the formation of any new phases in the solder joints. However, it has to be noted, that the TiO_2 nanoparticles were successfully mixed within the SAC305 as it was demonstrated by the TiO_2 peak in the XRD curves [20]. The increase of the peak intensities from CS-1 to CS-4 were mainly caused by the larger cross section surfaces due to the geometrical shape of the solder bumps. The differences of the peak intensities between the SAC305 and SAC305-TiO_2 can be explained by the increased heterogeneous nucleation of the phases. Since the doping of a system would help lower interfacial energy and thereby, promote the nucleation. The presence of non-interacting dispersoids such as TiO_2 in this case, helps the nucleation of favourable phases [21]. Therefore, TiO_2 not only prompt the formation of finer β-Sn grains, but also offers additional nucleation sites for the formation of refined Cu_6Sn_5 IMCs [9]. This could be the reason of the higher Cu_6Sn_5 peak intensities observed on the CS-4 of SAC305-TiO_2.

3.3 Morphology and elemental analysis

The significant differences between the Cu_6Sn_5 IMCs in the SAC305 and SAC305-TiO_2 solder joints can be seen in the micrographs (**Figure 4 and 5**). In the SAC305 solder joints, rod-like Cu_6Sn_5 IMCs are visible in CS-1, CS-2 and CS-3 (**Figure 4a-c**), as well as some white thread-like Ag_3Sn particles located around these larger rod-like Cu_6Sn_5 in CS-1 and CS-3. In CS-4 sample, the round-shaped Cu_6Sn_5 particles distributed sporadically across the surface with the presence of porosities (**Figure 4d**). In the SAC305-1.0T samples, the rod-like Cu_6Sn_5 IMCs are smaller with an average width of 9 µm (**Figure 5a-c**) in comparison to the SAC305 with 22 µm. Additionally, in the SAC305-1.0T samples, the Ag_3Sn IMC appeared in dot-like form instead of thread-like form as those observed in SAC305 samples. Here, the rounded Cu_6Sn_5 IMCs are more evenly distributed than they are in the SAC305 (**Figure 5d**). The presence of the previous phases on the surfaces of the cross sections was further validated by the subsequent scanned EDX (**Figure 4e and 5e**).

The rod-like Cu_6Sn_5 IMCs in CS1 – CS3 were attributed to the common faceted rod morphologies of the Cu_6Sn_5 which forms during normal undercooling nucleation [22]. The relatively larger Cu_6Sn_5 rods, as they can be seen in the centre of the solder bumps (e.g., CS-3) mainly formed due to the larger solidification area. The rounded IMCs observed in CS-4 are actually the top cross-section of the scallop type Cu_6Sn_5 IMC layer, which formed at the

solder/substrate interface [23]. The transformation of the thread-like Ag_3Sn to dot-like, was caused by the growth suppression, induced by the addition of TiO_2 nanoparticles [24]. A similar reduction on the crystal growth also affected the Cu_6Sn_5, as it can be seen in the SAC305-1.0T solder bumps. It has to be noted, that the addition of TiO_2 nanoparticle not only caused a higher density of simultaneous nucleation for the Cu_6Sn_5 and the absence of porosities, but also resulted in a more even distribution of the smaller-sized Cu_6Sn_5 particles at the CS-4 region in the SAC305-1.0T solder bumps [25].

3.4 Nanoindentation for hardness evaluations

A varied depth of penetration was observed on all cross-sections. Although the depth of penetration of the SAC305 (**Figure 6a-d**) were found to be relatively larger (from 3500 nm to 4000 nm) than at the SAC305-1.0T (from 3000 nm to 3500 nm) (**Figure 7a-d**). Both alloys showed gradual penetration reduction from CS-1 to CS-4 (**Figure 7a-d**). In comparison the results of CS-4 regions, SAC305-1.0T showed a smaller depth of penetration (3325 nm), than the SAC305 (3745 nm). In the hardness values, SAC305 showed only 1.28% increment from CS-1 (0.14012 GPa) to CS-4 (0.14192 GPa), while SAC305-1.0T had a substantial 25.9% improvement from 0.14077 GPa (at CS-1) to 0.17731 GPa (at CS-4).

The higher depth of penetration at the SAC305 alloy suggests that the applied force deformed this alloy more than it did in the case of SAC305-1.0T (**Table 2**). The increase of the deformation resistance across CS-1 to CS-4 in both alloys was also observed. This could be attributed to the higher nucleation of the harder Cu_6Sn_5 phases towards the CS-4 region due to the additional source of Cu (originated from the wiring of the FR4 substrate) [22]. The depth of penetration correlates with the hardness value as a result of the load-controlled condition upon indentation [26, 27]. This explains the relatively higher hardness values observed at the CS-4 region for both alloys. The distribution of the integrated TiO_2 nanoparticles in SAC305-1.0T also supports the dispersion strengthening mechanism [28]. As depicted from this study, the higher hardness values of the SAC305-1.0T were caused by the presence of TiO_2 nanoparticles, which had basically prevented the dislocation slipping and deformation along the grain boundaries [29].

Load-depth hysteresis comparison of the cross-sections can provide a better representation of the average hardness differences observed at the solder alloys (**Figure 8a-b**). The average values on the different cross-sections are also showed as the horizontal hardness profiles of the investigated alloys (**Figure 8c**). Although both alloys showed a progressive linear increase of the hardness values from CS-1 to CS-4 region, a more detailed observation

reveals a slightly higher increase at the SAC305-1.0T alloy than at the SAC305. The deviation of the curves at the SAC305-1.0T alloy (**Figure 8b**) towards the solder/substrate interface region was larger than at the SAC305 alloy (**Figure 8a**).

Additional Cu source from the wiring of the FR4 substrate enhances the formation of the Cu_6Sn_5 IMCs at the interface region [30]. In the SAC305-1.0T alloy, the additional nucleation sites provided by the non-interacting TiO_2 and the higher presence of the relatively hard Cu_6Sn_5 phases are probably related to the larger deviation of the hardness curves. As well as, the large deviation proves the influence of the integrated TiO_2 in refining the morphologies of the IMCs. The microstructure of the solder bumps at the CS-4 region showed higher density of the TiO_2 nanoparticles at the solder/substrate interface, and it caused the more dense Cu_6Sn_5 and Ag_3Sn networks in this region, which functioned as an entrapment for the TiO_2 nanoparticles [19].

3.5 Mechanism of horizontal hardness improvement of the SAC305-1.0TiO$_2$

The differences in the force distribution along the β-Sn and the IMC phases is illustrated on s schematics at the CS-2 (centre) cross-sections and at the CS-4 (lower) cross-section (**Figure 9 – 10**). The CS-2 cuts (located approximately in the middle of the solder bumps) consists of β-Sn matrix, thread-like Ag_3Sn and rod-like Cu_6Sn_5 phases. The CS-4 cuts (located at the scallop Cu_6Sn_5 IMC layer at the solder/substrate interface) consists of β-Sn matrix, dot-like Ag_3Sn and the rounded Cu_6Sn_5.

The SAC305 alloy contains larger IMC phases (Cu_6Sn_5 and Ag_3Sn as well) (**Figure 9a-b**). The favourable crystal growth resulted in not only larger grains, but the inhomogeneous distribution of the grains as well [31]. During the hardness testing, the applied force of the indenter distributed into the cross-section through dislocation movements along the grain boundaries of the β-Sn, Ag_3Sn and the rod-like Cu_6Sn_5 particles. In the case of CS-2, the applied force penetrated easily into the cross-section, due to the less obstacles on the distribution networks (**Figure 9a**). At the CS-4 cross-section, the relatively higher presence of rounded Cu_6Sn_5 (due to the Cu_6Sn_5 IMC layer) provided barriers for the force distribution along the grain boundaries (**Figure 9b**).

The addition of the TiO_2 nanoparticles significantly refined the Ag_3Sn and Cu_6Sn_5 particles (**Figure 10a-b**) and the heterogonous nucleation provided more homogeneous distribution of the IMC phases [32]. Thus, at the CS-2 cross-section, the dislocation movements induced by the applied force faced to higher obstacles during the force distribution due to the finer and well distributed Ag_3Sn and Cu_6Sn_5 particles. Similarly, at the CS-4 l cross-section,

the smaller rounded Cu_6Sn_5 particles also caused higher resistance for the dislocation movements. Therefore, it can be concluded that the finer Ag_3Sn and Cu_6Sn_5 grain structure is responsible for the grain boundary strengthening mechanism and resulted in the improved mechanical properties and deformation resistance of SAC305-1.0T alloy [33, 34].

4. Conclusions

The SAC305 solder alloy reinforced with 1.0 wt. % of TiO_2 nanoparticles was prepared and the mechanical properties of the composite solder alloy was analysed and compared to the base SAC305. The XRD analysis showed that the TiO_2 nanoparticles were successful blended into the SAC305 solder paste. The slight increase of the TiO_2 peak intensity at the lower cross sections suggested a favourable distribution of the TiO_2 nanoparticles at the particular region. SEM micrographs about the solder/substrate interface showed that the SAC305-1.0T solder composite contains dot-like Ag_3Sn, while the SAC305 contains needle-like Ag_3Sn. In addition, the presence of TiO_2 nanoparticles resulted in the size reduction of Cu_6Sn_5 phases. The average hardness value on all horizontal cross-sections was found to be higher in the case of the composite SAC305-1.0T solder alloy than in the case of the SAC305 alloy. The refined Ag_3Sn and Cu_6Sn_5 IMC phases due to the presence of the TiO_2 nanoparticles significantly restrained the dislocation movements during mechanical load which is responsible for improving the hardness of the solder joints.

Acknowledgements

Siti Shareeda Binti Mohd Nasir thanked the Universiti Teknologi Mara (UiTM). Muhamad Zamri Yahaya and Ahmad Azmin Mohamad appreciate the financial support provided by the FRGS grant 203.PBahan.6071377 (Ref: FRGS/1/2017/TK05/USM/02/2). Balázs Illés thanks the financial support provided by the National Research, Development and Innovation Office – NKFIH, FK 127970.

References

[1] A. El-Daly, A. Hammad, G. Al-Ganainy, M. Ragab, Properties enhancement of low Ag-content Sn–Ag–Cu lead-free solders containing small amount of Zn, J. Alloy Compd. 614 (2014) 20-28.

[2] S. Chang, C. Jain, T. Chuang, L. Feng, L. Tsao, Effect of addition of TiO 2 nanoparticles on the microstructure, microhardness and interfacial reactions of Sn3. 5AgXCu solder, Mater. Design 32(10) (2011) 4720-4727.

[3] C. Chuang, L. Tsao, H. Lin, L. Feng, Effects of small amount of active Ti element additions on microstructure and property of Sn3. 5Ag0. 5Cu solder, Mat. Sci. Eng. A-Struct. 558 (2012) 478-484.

[4] O.M. Abdelhadi, L. Ladani, IMC growth of Sn-3.5 Ag/Cu system: combined chemical reaction and diffusion mechanisms, J. Alloy Compd. 537 (2012) 87-99.

[5] A. Fawzy, S. Fayek, M. Sobhy, E. Nassr, M. Mousa, G. Saad, Tensile creep characteristics of Sn–3.5 Ag–0.5 Cu (SAC355) solder reinforced with nano-metric ZnO particles, Mat. Sci. Eng. A-Struct. 603 (2014) 1-10.

[6] J. Shen, Y. Liu, Y. Han, Y. Tian, H. Gao, Strengthening effects of ZrO_2 nanoparticles on the microstructure and microhardness of Sn-3.5Ag lead-free solder, J. Electron. Mater. 35(8) (2006) 1672-1679.

[7] Y. Tang, G. Li, Y. Pan, Effects of TiO 2 nanoparticles addition on microstructure, microhardness and tensile properties of Sn–3.0 Ag–0.5 Cu–xTiO 2 composite solder, Mater. Design 55 (2014) 574-582.

[8] L. Tsao, An investigation of microstructure and mechanical properties of novel Sn3. 5Ag0. 5Cu–XTiO 2 composite solders as functions of alloy composition and cooling rate, Mat. Sci. Eng. A-Struct. 529 (2011) 41-48.

[9] L. Tsao, C. Huang, C. Chung, R. Chen, Influence of TiO 2 nanoparticles addition on the microstructural and mechanical properties of Sn0. 7Cu nano-composite solder, Mat. Sci. Eng. A-Struct. 545 (2012) 194-200.

[10] J. Shen, Y.C. Chan, Research advances in nano-composite solders, Microelectron. Reliab. 49(3) (2009) 223-234.

[11] A. Sharma, B. Baek, J.P. Jung, Influence of La2O3 nanoparticle additions on microstructure, wetting, and tensile characteristics of Sn–Ag–Cu alloy, Mater. Design 87 (2015) 370-379.

[12] A.K. Gain, T. Fouzder, Y.C. Chan, W.K. Yung, Microstructure, kinetic analysis and hardness of Sn–Ag–Cu–1 wt% nano-ZrO2 composite solder on OSP-Cu pads, J. Alloy. Compd. 509(7) (2011) 3319-3325.

[13] L. Tsao, S. Chang, C. Lee, W. Sun, C. Huang, Effects of nano-Al2O3 additions on microstructure development and hardness of Sn3. 5Ag0. 5Cu solder, Materials & Design 31(10) (2010) 4831-4835.

[14] A. Geranmayeh, R. Mahmudi, M. Kangooie, High-temperature shear strength of lead-free Sn–Sb–Ag/Al2O3 composite solder, Mat. Sci. Eng. A-Struct. 528(12) (2011) 3967-3972.

[15] A. El-Daly, W. Desoky, T. Elmosalami, M. El-Shaarawy, A. Abdraboh, Microstructural modifications and properties of SiC nanoparticles-reinforced Sn–3.0 Ag–0.5 Cu solder alloy, Mater. Design 65 (2015) 1196-1204.
[16] X. Wang, Y. Liu, C. Wei, H. Gao, P. Jiang, L. Yu, Strengthening mechanism of SiC-particulate reinforced Sn–3.7 Ag–0.9 Zn lead-free solder, J. Alloy. Compd. 480(2) (2009) 662-665.
[17] S. Chang, C. Jain, T. Chuang, L. Feng, L. Tsao, Effect of addition of TiO2 nanoparticles on the microstructure, microhardness and interfacial reactions of Sn3. 5AgXCu solder, Materials & Design 32(10) (2011) 4720-4727.
[18] L. Tsao, S. Chang, Effects of nano-TiO_2 additions on thermal analysis, microstructure and tensile properties of Sn3.5Ag0.25Cu solder, Mater. Design 31(2) (2010) 990-993.
[19] M.Z. Yahaya, F.C. Ani, Z. Samsudin, S. Sahin, M.Z. Abdullah, A.A. Mohamad, Hardness profiles of Sn-3.0 Ag-0.5 Cu-TiO2 composite solder by nanoindentation, Mat. Sci. Eng. A-Struct. 669 (2016) 178-186.
[20] L. Tsao, S. Cheng, C. Chen, T.-Y. Chen, Effect of nano-TiO2 particles and cooling rate on the thermal, microstructure and mechanical properties of novel low-ag Sn1. 5Sb1Ag solders, Mat. Sci. Eng. A-Struct. 658 (2016) 159-166.
[21] S. Jin, M. McCormack, Dispersoid additions to a Pb-free solder for suppression of microstructural coarsening, J. Electron. Mater. 23(8) (1994) 735-739.
[22] J. Xian, Z. Ma, S. Belyakov, M. Ollivier, C. Gourlay, Nucleation of tin on the Cu6Sn5 layer in electronic interconnections, Acta Mater. 123 (2017) 404-415.
[23] L. Tsao, Suppressing effect of 0.5 wt.% nano-TiO 2 addition into Sn–3.5 Ag–0.5 Cu solder alloy on the intermetallic growth with Cu substrate during isothermal aging, J. Alloy Compd. 509(33) (2011) 8441-8448.
[24] A. Roshanghias, A. Kokabi, Y. Miyashita, Y. Mutoh, I. Ihara, R.G. Fatt, H. Madaah-Hosseini, Nanoindentation creep behavior of nanocomposite Sn-Ag-Cu solders, J. Electron. Mater. 41(8) (2012) 2057-2064.
[25] S. Xu, Y.C. Chan, K. Zhang, K. Yung, Interfacial intermetallic growth and mechanical properties of carbon nanotubes reinforced Sn3. 5Ag0. 5Cu solder joint under current stressing, J. Alloy Compd. 595 (2014) 92-102.
[26] G. Xiao, G. Yuan, C. Jia, X. Yang, Z. Li, X. Shu, Strain rate sensitivity of Sn–3.0 Ag–0.5 Cu solder investigated by nanoindentation, Mat. Sci. Eng. A-Struct. 613 (2014) 336-339.
[27] M.Z. Yahaya, A.A. Mohamad, Hardness testing of lead-free solders: a review, Solder. Surf. Mt. Tech. 29(4) (2017) 203-224.

[28] X. Hu, Y. Qiu, X. Jiang, Y. Li, Effect of Cu 6 Sn 5 nanoparticle on thermal behavior, mechanical properties and interfacial reaction of Sn3. 0Ag0. 5Cu solder alloys, J. Mater. Sci-Mater. El. 29(18) (2018) 15983-15993.
[29] L. Xu, S. Zhang, H. Jing, L. Wang, J. Wei, X. Kong, Y. Han, Indentation Size Effect on Ag Nanoparticle-Modified Graphene/Sn-Ag-Cu Solders, J. Electron. Mater. 47(1) (2018) 612-619.
[30] V.M.F. Marques, C. Johnston, P.S. Grant, Microstructural evolution at Cu/Sn–Ag–Cu/Cu and Cu/Sn–Ag–Cu/Ni–Au ball grid array interfaces during thermal ageing, J. Alloy. Compd. 613 (2014) 387-394.
[31] L. Tsao, M. Wu, S. Chang, Effect of TiO2 nanoparticles on the microstructure and bonding strengths of Sn0. 7Cu composite solder BGA packages with immersion Sn surface finish, J. Mater. Sci-Mater. El. 23(3) (2012) 681-687.
[32] M. Ramli, N. Saud, M.M. Salleh, M.N. Derman, R.M. Said, Effect of TiO2 additions on Sn-0.7 Cu-0.05 Ni lead-free composite solder, Microelectron. Reliab. 65 (2016) 255-264.
[33] Y. Shi, J. Liu, Z. Xia, Y. Lei, F. Guo, X. Li, Creep property of composite solders reinforced by nano-sized particles, J. Mater. Sci-Mater. El. 19(4) (2008) 349-356.
[34] L. Tsao, S. Chang, C. Lee, W. Sun, C. Huang, Effects of nano-Al_2O_3 additions on microstructure development and hardness of Sn3.5Ag0.5Cu solder, Mater. Design 31(10) (2010) 4831-4835.

Figures:

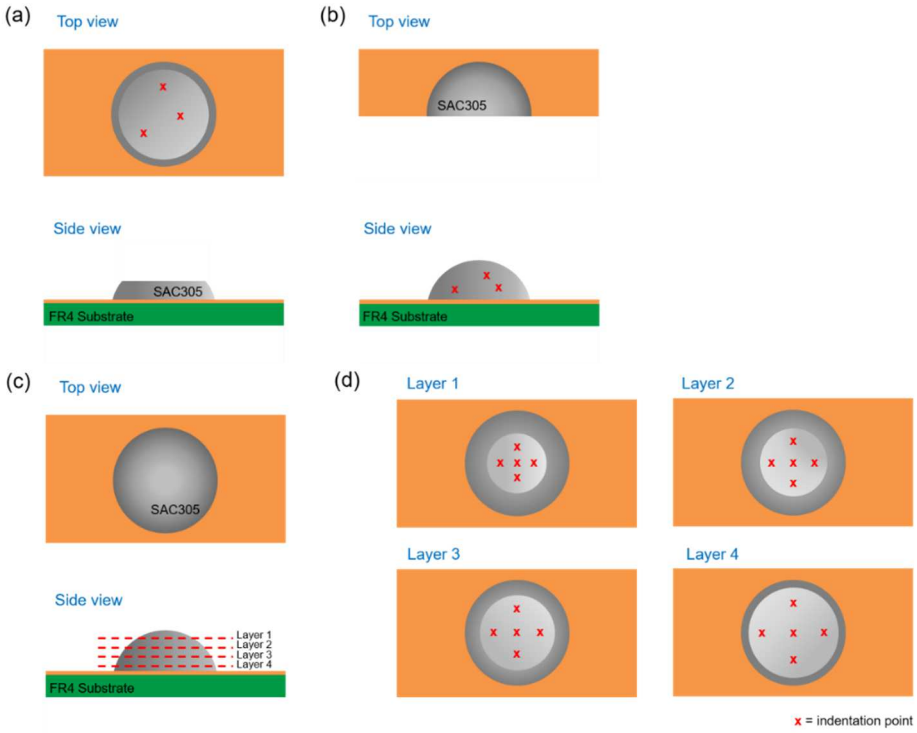

Figure 1: Schematic of the (a) horizontal indentation (b) vertical indentation (c) multilayer horizontal indentation and (d) indentation of individual layer in (c).

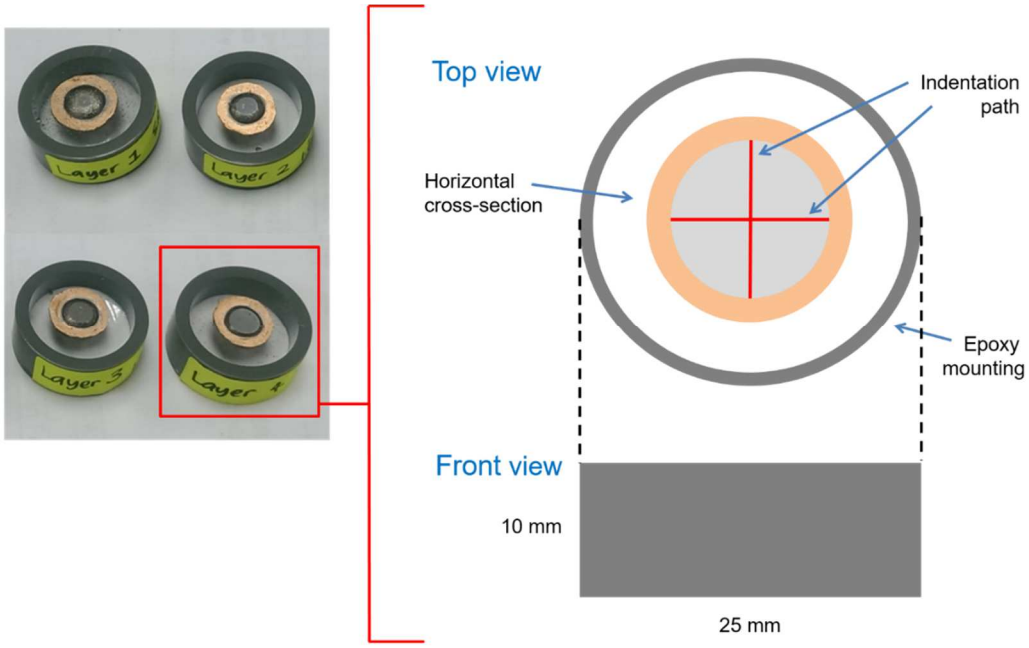

Figure 2: Schematic of the indentation path of the nanoindentation on the horizontal cross-sections.

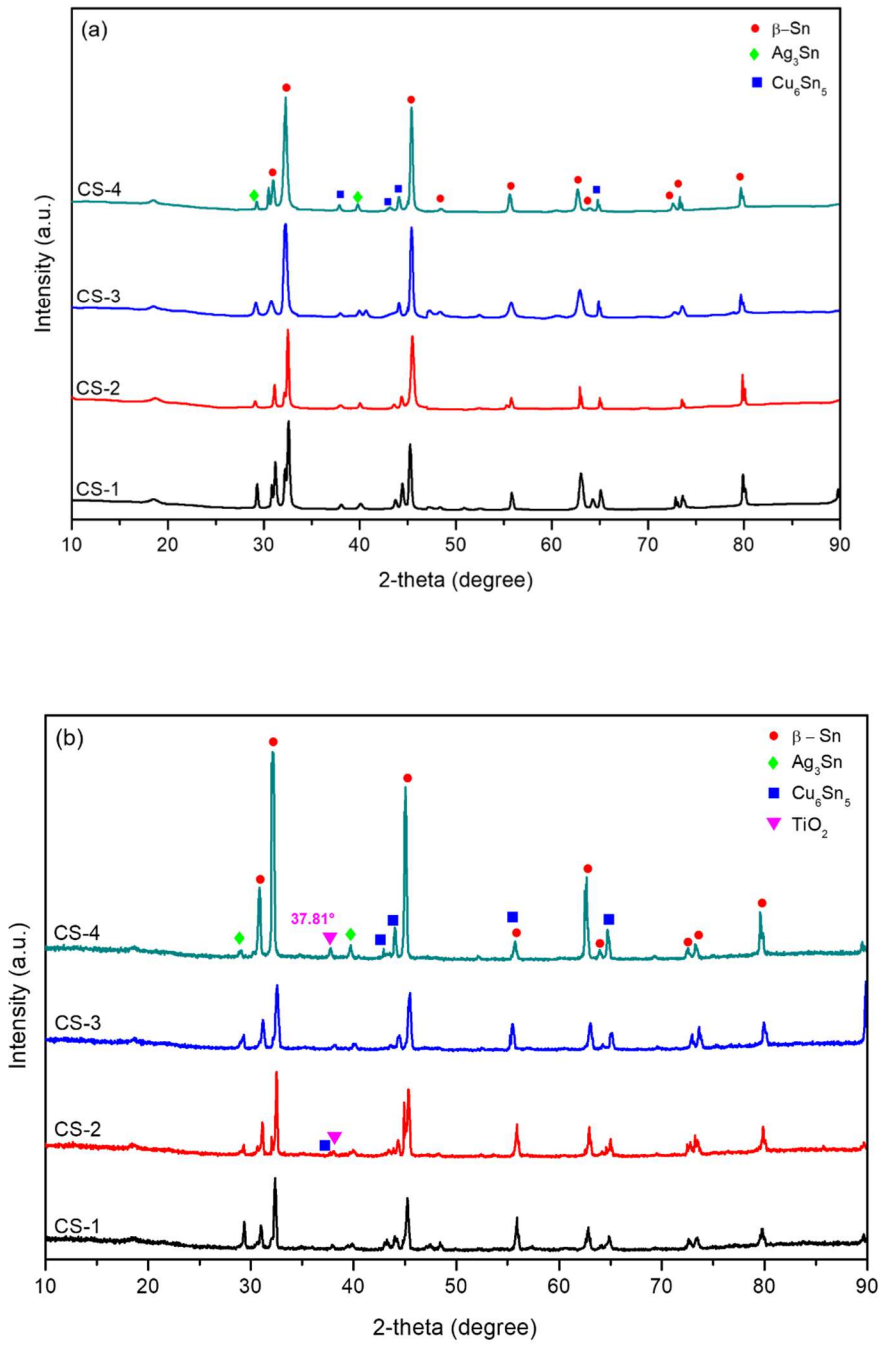

Figure 3: XRD curves of the (a) SAC305 and (b) SAC305-1.0T at different horizontal layers.

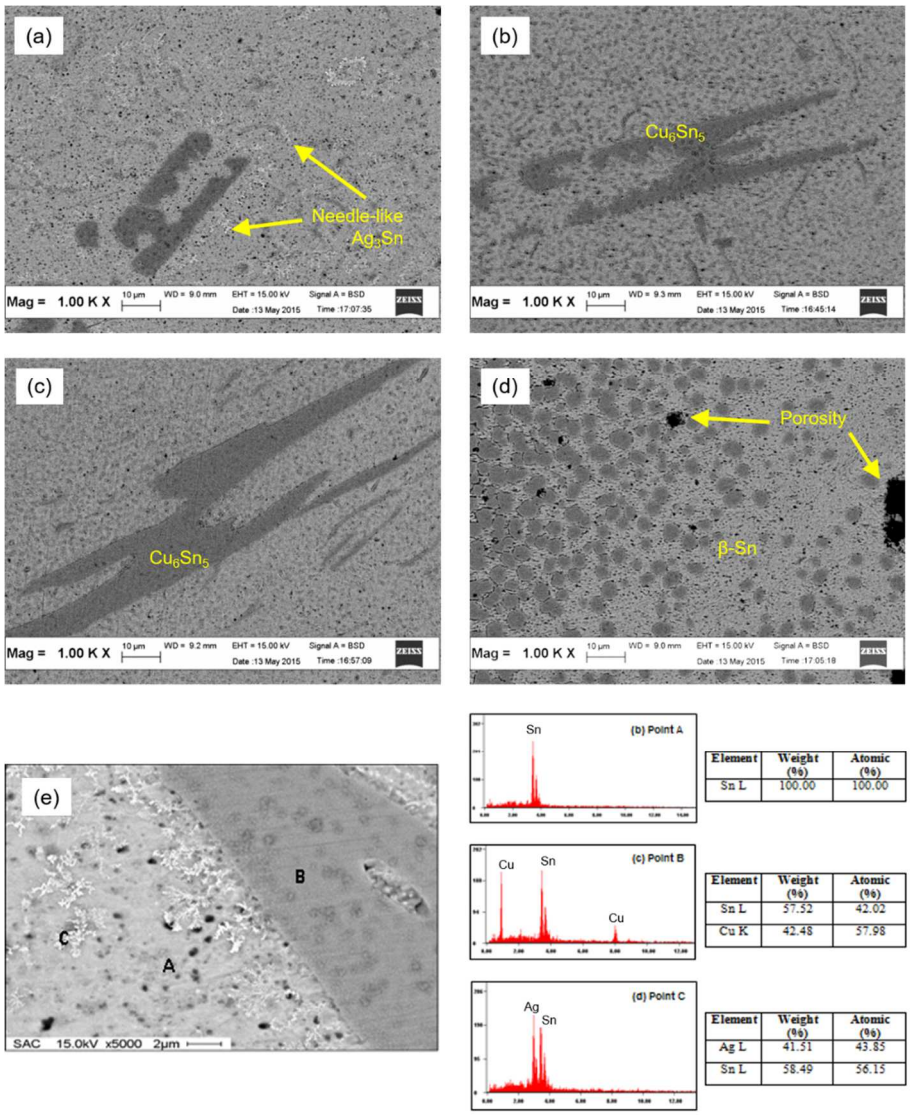

Figure 4: Morphology behaviour of pure SAC305 solder alloy at (a) CS-1 region, (b) CS-2 region, (c) CS-3 region, (d) CS-4 region and (e) the micrographs of CS-3 used for the EDX.

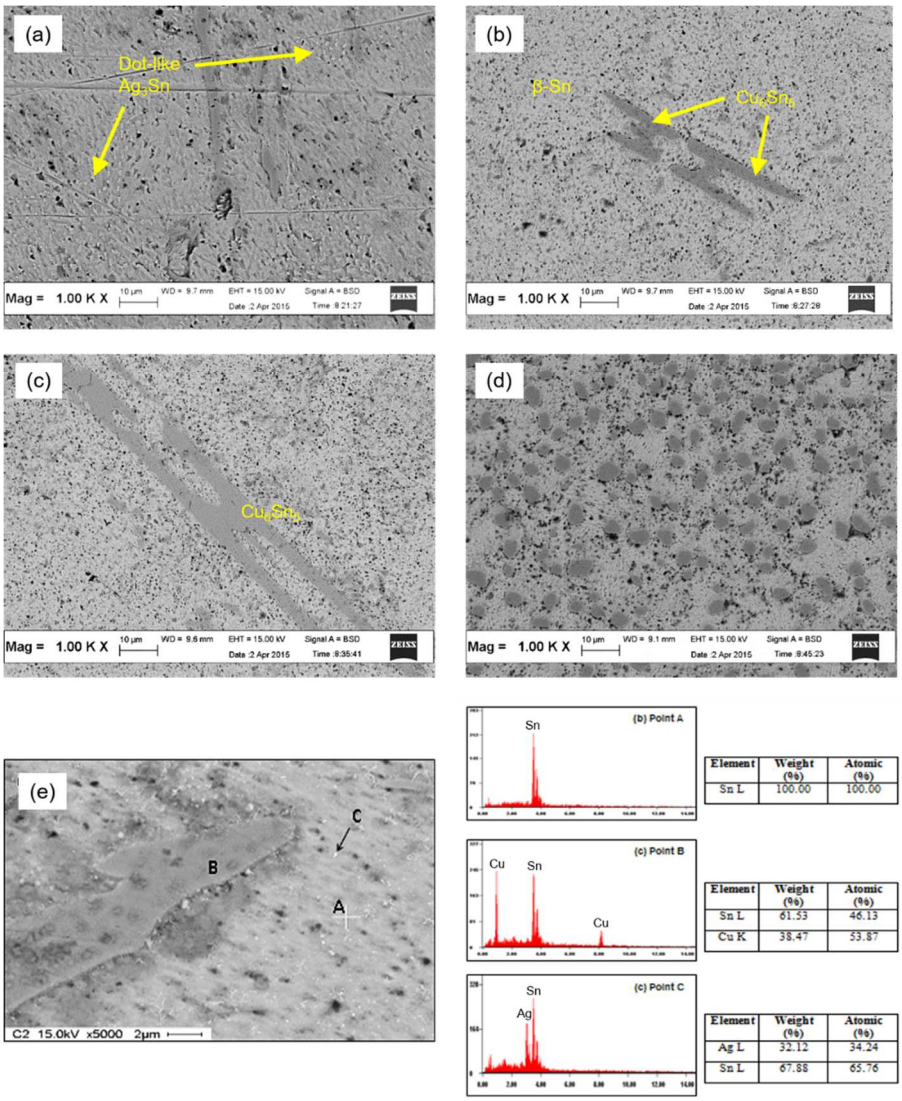

Element	Weight (%)	Atomic (%)
Sn L	100.00	100.00

Element	Weight (%)	Atomic (%)
Sn L	61.53	46.13
Cu K	38.47	53.87

Element	Weight (%)	Atomic (%)
Ag L	32.12	34.24
Sn L	67.88	65.76

Figure 5: Morphology of SAC305-1.0T solder alloy at (a) CS-1 region, (b) CS-2 region, (c) CS-3 region, (d) CS-4 region and (e) the micrographs of CS-3 used for the EDX.

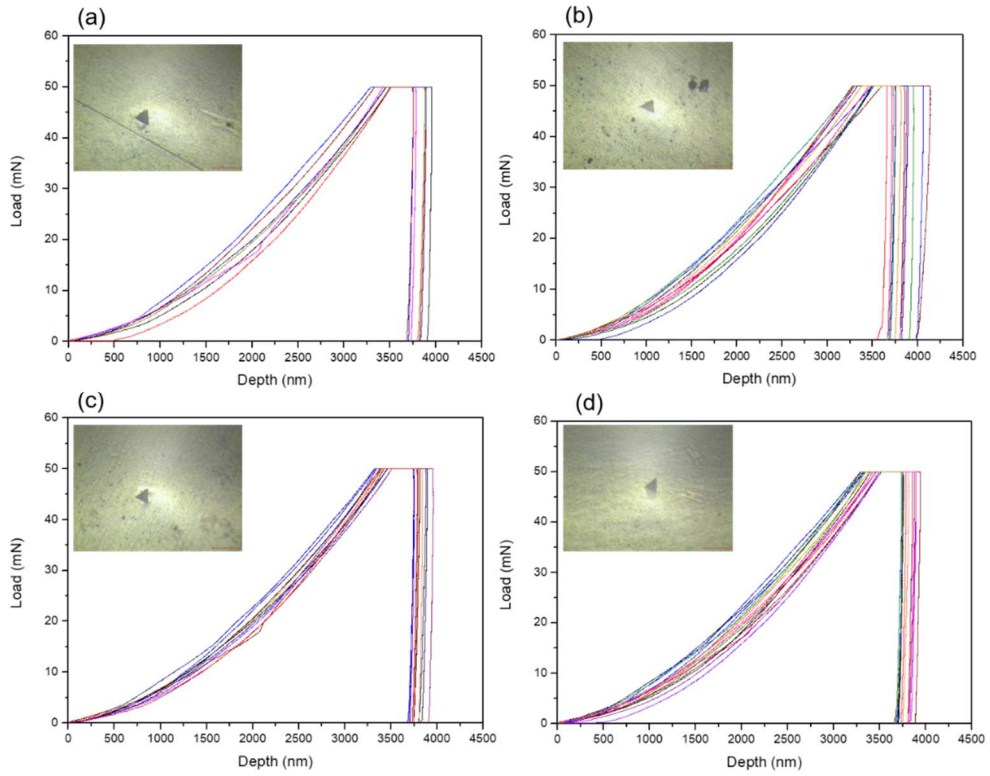

Figure 6: Indentation load-depth curves of the SAC305 solder alloy at (a) CS-1, (b) CS-2, (c) CS-3 and (d) CS-4 regions.

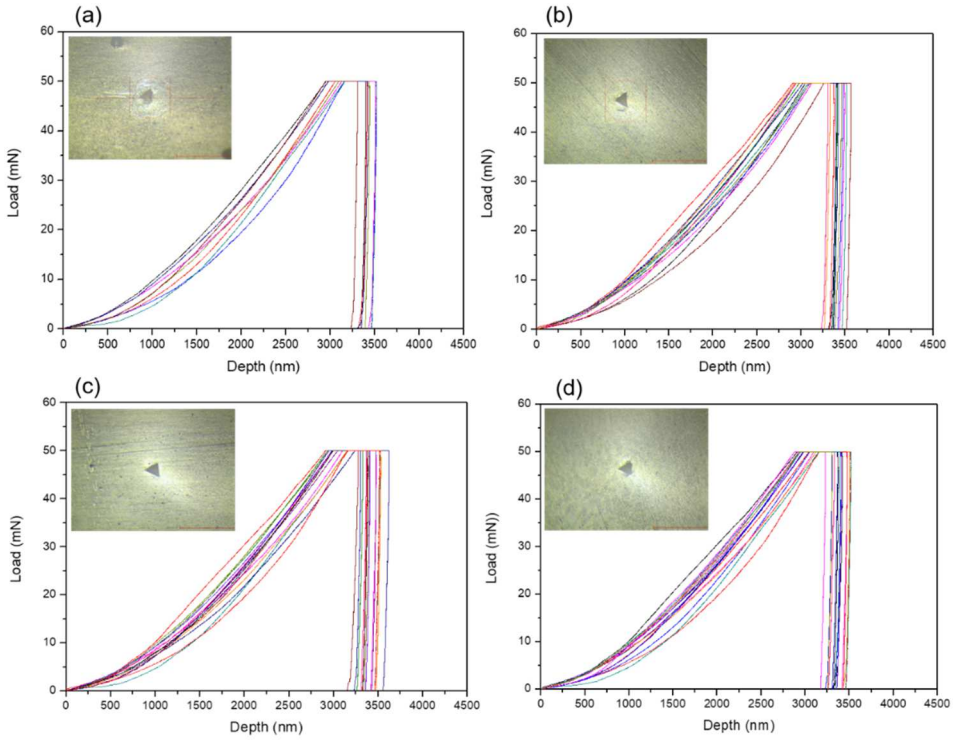

Figure 7: Indentation load-depth curves of the SAC305-1.0T solder alloy at (a) CS-1, (b) CS-2, (c) CS-3 and (d) CS-4 regions.

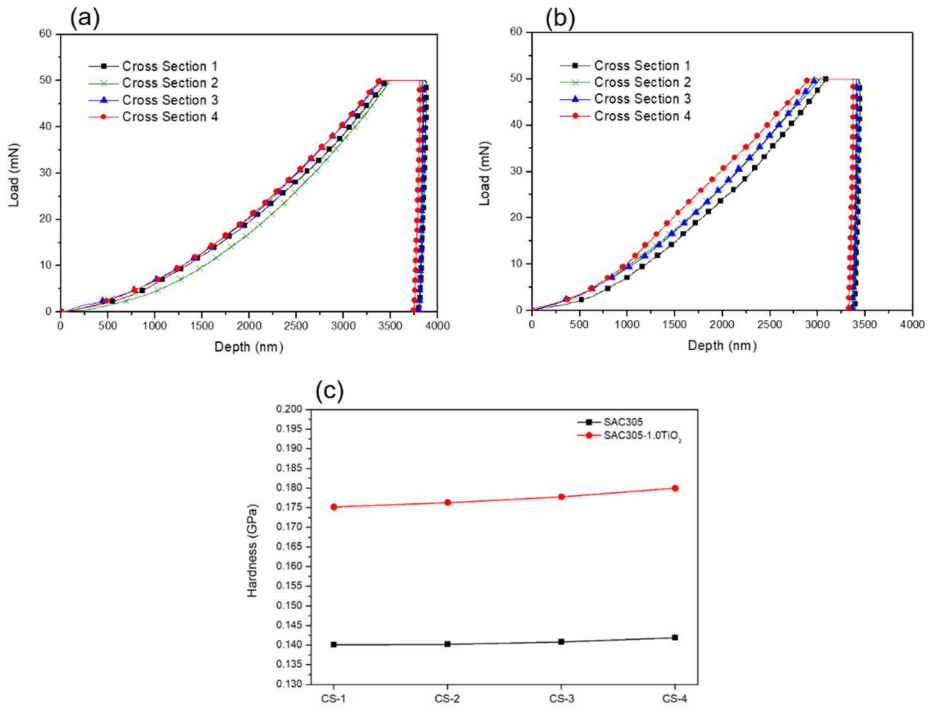

Figure 8: Load-depth hysteresis comparison of the cross-sections (a) SAC305 solder alloy, (b) SAC305-1.0TiO_2 solder alloy; and (c) hardness profiles of the solder alloys.

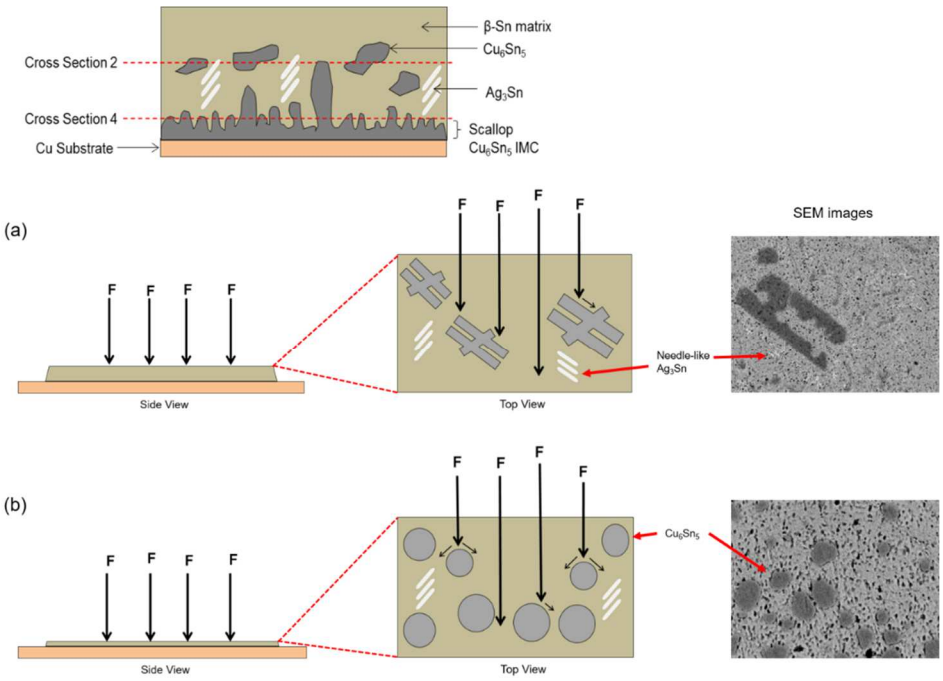

Figure 9: Side and top view of the force distribution in the SAC305 solder bump at (a) CS-2 and (b) CS-4 regions.

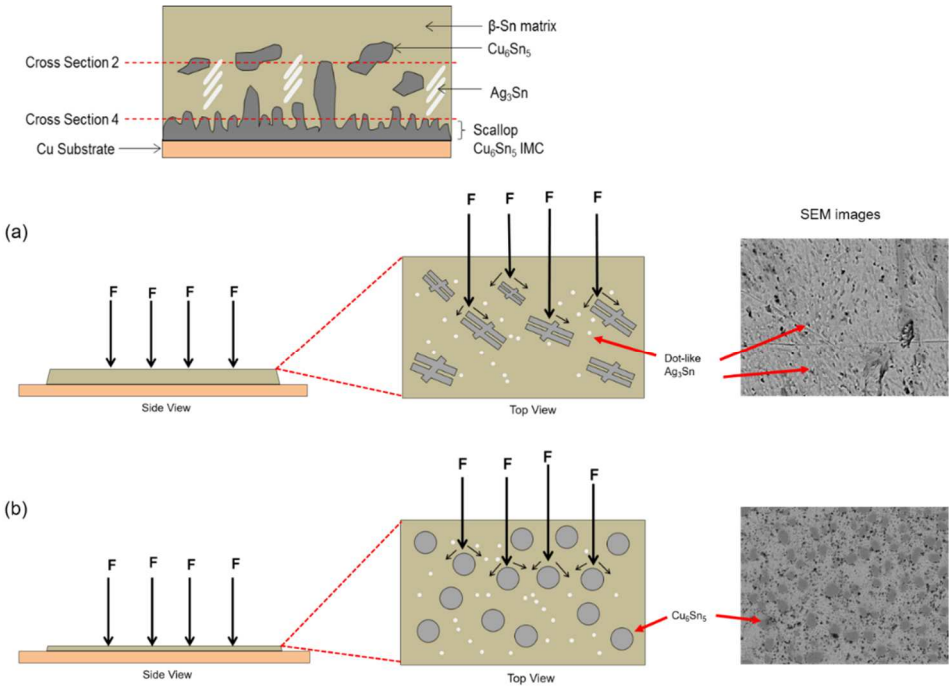

Figure 10: Side and top view of the force distribution in SAC305-1.0TiO_2 solder bump at (a) CS-2 and (b) CS-4 regions.

Tables:

Table 1: Surface diameter and height of the horizontal cross-sections of the samples

Cross Section	Sample Designation	Surface diameter (mm)	Height (mm)
1	CS-1	2	0.85
2	CS-2	3	0.60
3	CS-3	4	0.35
4	CS-4	5	0.10

Table 2: Average depth displacement and average hardness value of the cross- sections.

	SAC305		SAC305-1.0T	
Cross Section	Average depth displacement (nm)	Average Hardness Values (GPa)	Average depth displacement (nm)	Average Hardness Values (GPa)
CS-1	3748	0.14012	3458	0.17521
CS-2	3621	0.14023	3405	0.17632
CS-3	3566	0.14082	3248	0.17778
CS-4	3501	0.14192	3124	0.17996